Radio Sources in the 2dF Galaxy Redshift Survey
I. Radio Source Populations*

Elaine M. Sadler[1], V. J. McIntyre[1],
C. A. Jackson[1] and R. D. Cannon[2]

[1]School of Physics, University of Sydney, NSW 2006, Australia
ems@physics.usyd.edu.au, vjm@physics.usyd.edu.au, cjackson@physics.usyd.edu.au
[2]Anglo-Australian Observatory, PO Box 296, Epping, NSW 2121, Australia
rdc@aaoepp.aao.gov.au

Abstract: We present the first results from a study of the radio continuum properties of galaxies in the 2dF Galaxy Redshift Survey, (2dFGRS) based on thirty 2dF fields covering a total area of about $100\,\mathrm{deg}^2$. About $1\cdot5\%$ of galaxies with $b_{\mathrm{J}} < 19\cdot4$ mag. are detected as radio continuum sources in the NRAO VLA Sky Survey (NVSS). Of these, roughly 40% are star-forming galaxies and 60% are active galaxies (mostly low-power radio galaxies and a few Seyferts). The combination of 2dFGRS and NVSS will eventually yield a homogeneous set of around 4000 radio-galaxy spectra, which will be a powerful tool for studying the distribution and evolution of both AGN and starburst galaxies out to $z \sim 0\cdot3$.

Keywords: radio continuum: galaxies — galaxies: distances and redshifts — galaxies: active — galaxies: starburst

1 Introduction

A new generation of sensitive large-area radio-source surveys at milliJanksy levels (1 Jy = 10^{-26} W m^{-2} Hz^{-1}) is now becoming available. They include the FIRST survey (Becker, White & Helfand 1995), WENSS (Rengelink et al 1997), NVSS (Condon et al. 1998) and SUMSS (Bock, Large & Sadler 1999). These surveys offer some important advantages for cosmological studies—they reach sufficiently high source densities that detection of large-scale structure is possible (Cress et al. 1996; Magliocchetti et al. 1998), and also probe a second cosmologically-significant radio source population, that of star-forming galaxies, which are rarely seen in strong-source surveys.

Deep radio surveys of a few small areas of sky at $1\cdot4$ GHz (Condon 1984; Windhorst et al. 1985; see also Condon 1992) have shown that there are two distinct populations of extragalactic radio sources. Over 95% of radio sources above about 50 mJy are classical radio galaxies and quasars (median redshift $z \sim 1$) powered by active galactic nuclei (AGN), while the remainder are identified with star-forming galaxies (median $z \sim 0\cdot1$). The fraction of star-forming galaxies increases rapidly below 10 mJy, and below 1 mJy they begin to be the dominant population.

The scientific return from radio continuum surveys is enormously increased if the optical counterparts of the radio sources can be identified and their redshift distribution measured. In the past, this has been a slow and tedious process which could only be carried out for relatively small samples. However, the Anglo-Australian Observatory's Two-degree Field (2dF) spectrograph now makes it possible to carry out spectroscopy of several hundred galaxies simultaneously. Here, we describe the first step in this process—the identification of faint radio-source counterparts among galaxies whose spectra have been obtained in the 2dF Galaxy Redshift Survey.

The 2dFGRS (Colless 1999; Maddox 1998) is a large-scale survey of 250,000 galaxies covering 2000 square degrees in the southern hemisphere. The survey is designed to be almost complete down to a limiting apparent magnitude of $b_{\mathrm{J}} = 19\cdot4$. The median redshift of the galaxies is about $0\cdot1$
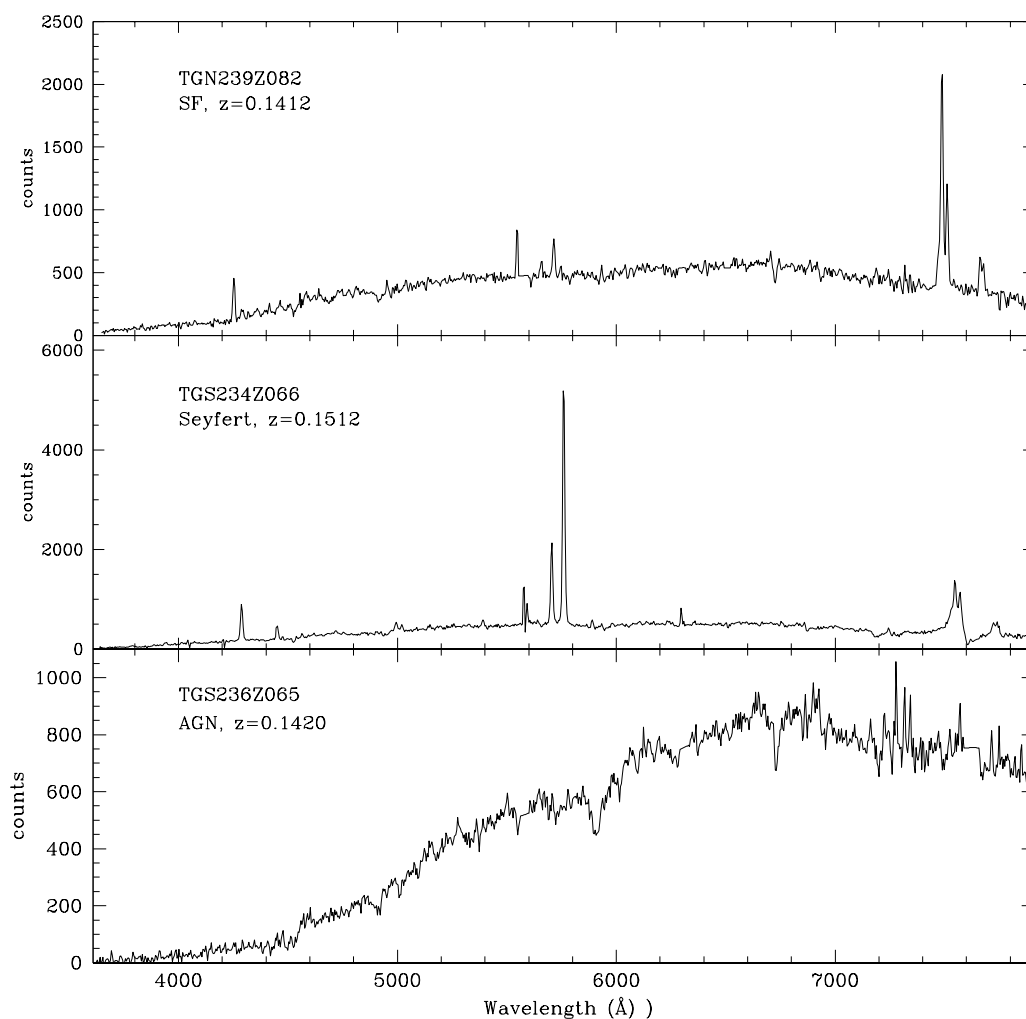
Figure 1—Spectra of three 2dFGRS radio sources, showing the three main spectral classes: (*top*) A star-forming galaxy, TGN239Z082, with strong Balmer emission lines of Hα $\lambda6563$ and Hβ $\lambda4861$, as well as weaker emission lines of [SII] $\lambda6716,6731$, [NII] $\lambda6583$, [OIII] $\lambda4959,5007$ and [OII] $\lambda3727$; (*middle*) an emission-line AGN, TGS234Z066, with a Seyfert-like spectrum which has broad Hα emission and [OIII] much stronger than Hβ; and (*bottom*) A radio galaxy, TGS236Z065, with an absorption-line spectrum typical of giant elliptical galaxies.

and the great majority have $z < 0\cdot3$. Spectra are being obtained using the 2dF multi-object fibre optic spectroscopic system on the $3\cdot9$ m Anglo-Australian Telescope (AAT) (Lewis, Glazebrook & Taylor 1998; Smith & Lankshear 1998). The 2dF enables the AAT to obtain spectra for 400 objects simultaneously, spread over a field which is two degrees in diameter. The survey will cover two large strips of sky at high Galactic latitude, one each in the southern and northern Galactic hemispheres, plus outlying random fields in the south. The first test data were obtained in 1997 and the survey is expected to be substantially complete by the end of 2000.

This paper presents the first results from what will eventually be a much larger study. When the 2dFGRS is complete, it will yield around 4000 good-quality spectra of galaxies associated with faint radio sources—by far the largest sample of radio-galaxy spectra ever compiled. Our aim in this paper is to present a first, qualitative exploration

of the faint radio source population as observed by 2dF and the NVSS.

Throughout this paper, we use $H_0 = 75$ km s^{-1} Mpc^{-1} and $q_0 = 0\cdot5$.

2 The Optical Data

Our data set comprises the thirty fields observed by the 2dFGRS team in November 1997 and January 1998. Twenty-three of these are in the southern Galactic hemisphere and the other seven in the north. They include a total of 8362 target galaxies brighter than $b_{\rm J}$ magnitude $19\cdot4$.

Although each 2dF field covers about $3\cdot14$ square degrees, the total effective area covered by the 30 fields is somewhat less than 90 square degrees because there is some overlap between adjacent fields. Also, the fractional completeness of this early sample varies substantially from field to field. In many fields about 30% of the fibres were allocated to targets in a parallel QSO survey; the 2dFGRS uses a flexible tiling algorithm to deal with this

and with the intrinsic variations in target density across the sky. When complete, the GRS will yield spectra for around 95% of all galaxies in the input catalogue. The current sample has variable levels of completeness (in terms of the surface distribution of all galaxies brighter than $b_J = 19 \cdot 4$ mag.), though there should be no systematic effects depending on the magnitude, redshift or other properties of the galaxies.

The standard observing pattern for the 2dFGRS is a set of three consecutive 20-minute exposures per field, together with calibration arcs and flat fields. The total exposure time is well-matched to the time required to reconfigure a second set of fibres for the next observation. Up to 380 galaxies can be observed simultaneously, with some 20 fibres allocated to sky. In many fields, however, the total number of galaxies is closer to 250 since a deep QSO survey is being carried out in parallel with the galaxy redshift survey.

Using gratings of 300 lines per mm, the 2dFGRS spectra cover the wavelength range 3800 Å to 8000 Å at a resolution of about 10 Å. Most spectra have a signal-to-noise ratio (S/N) of 10 (per 4 Å pixel) or better. Reliable redshifts are obtained for up to 95% of the targets in good observing conditions; the survey average is currently about 90% (Folkes et al. 1999). About 5% of the targets are found to be foreground stars; the original selection was for objects which appeared non-stellar in digitised data from UK Schmidt Telescope sky survey photographs, using a conservative criterion to minimise the number of galaxies missed.

Figure 1 shows three spectra from the survey, and gives an idea of the typical quality of 2dFGRS spectra for galaxies with redshifts around $z = 0 \cdot 15$ and b_J magnitudes in the range $17 \cdot 6$–$18 \cdot 9$.

3 The Radio Data

The NRAO VLA Sky Survey (NVSS; Condon et al. 1998) is a $1 \cdot 4$ GHz (20 cm) radio imaging survey of the entire sky north of declination $-40°$. The survey catalogue contains sources as weak as $2 \cdot 5$ mJy, and is essentially complete above $3 \cdot 5$ mJy.

We used the NVSS source catalogue to identify candidate radio-emitting galaxies in the 2dFGRS. Subsets of the NVSS catalogue were extracted to match the RA and Dec range covered by each of the 2dF fields. The NVSS source density is roughly 60 per square degree, so each of these sub-catalogues contained about 200 radio sources. At this stage, we did not attempt to identify 'double' NVSS sources. However, we estimate [using an algorithm similar to that adopted by Magliocchetti et al. (1998) for identifying double radio sources in the FIRST survey] that these represent only a small fraction of NVSS sources (of order 1%), so the presence of double sources does not significantly affect our results in this small sample.

We compared the NVSS and 2dFGRS catalogues for each field and identified the galaxies for which there is a candidate radio 'match', i.e. an NVSS radio source lying within 15 arcsec of the position of a 2dF galaxy. The 15 arcsec limit was chosen because our earlier Monte Carlo tests using the COSMOS database suggested that most candidate matches of *bright* galaxies (i.e. $b_J < 19 \cdot 4$ mag.) with radio–optical separation up to 10 arcsec are real associations, together with a substantial fraction of those with offsets of 10–15 arcsec.

The uncertainty in the NVSS radio source positions increases from a 1σ error of 1–2 arcsec at 10 mJy to 4–5 arcsec (and occasionally up to 10 arcsec) for the faintest (2–3 mJy) sources (Condon et al. 1998). In addition, centroiding of bright radio sources with extended radio structure can be somewhat uncertain and may make optical identification difficult. Determining the optical centroid also becomes imprecise for large nearby galaxies. In these cases, overlaying the radio contours on an optical image usually makes it clear whether or not the candidate ID is correct.

We found a total of 127 candidate matches in the 30 fields studied, i.e. $1 \cdot 5\%$ of the 8362 2dF galaxies in the survey area. Of these, 99 had radio–optical offsets of less than 10 arcsec.

We also ran the matching program twice more, offsetting all the radio positions by 3 and 5 arcmin. Any matches produced from this 'off-source' catalogue should be chance coincidences, allowing us to estimate the number of matches expected purely by chance. Table 1 lists the results of this test, and shows the distribution of the offset D (the difference between radio and optical positions) for matches found in the 'on-source' and 'off-source' tests.

Table 1.   Comparison of on-source and off-source matches as a function of radio–optical offset D

'Off-source' data are for matches where the radio-source positions were offset in declination by 3 arcmin (Off 3) and 5 arcmin (Off 5)

D (arcsec)	No. of matches On	Off 3	Off 5	Predicted counts	Probability that match is real
0–2·5	34	3	0	1	96%
2·5–5·0	29	2	1	2	95%
5·0–10·0	36	6	8	9	81%
10·0–15·0	28	12	13	15	55%

A further check comes from predicting the expected number of chance coincidences, based on the average surface densities of objects. Since 15 arcsec is 1/240 of the 1 degree radius of each 2dF field, and there are about 60 NVSS sources per square degree, the chance that a given GRS target will fall within 15 arcsec of an unrelated radio source is about $60 \times \pi/240^2$ (the resolution of the NVSS is such that at most one

Table 2.   Galaxies with $\Delta < 10''$ and good-quality spectra

Field	ID	Offset (arcsec)	$B(J)$ (mag)	z	$S_{1\cdot4}$ (mJy)	IRAS S_{60} (Jy)	Spectral class
166s	TGS166Z108	6·7	17·2	0·0801	3·0	0·297	SF
203s	TGS203Z019	2·4	18·9	0·2358	85·1		AGN(abs)
203s	XGS202Z238	0·9	18·1	0·1389	90·5		AGN(abs)
204s	TGS204Z102	1·8	16·8	0·0759	3·2		AGN(abs)
204s	TGS204Z037	1·8	19·4	0·2643	54·0		AGN(E+[OIII]em)
206s	TGS206Z164	8·8	14·6	0·0255	2·9	0·293	SF
206s	TMS206Z015	1·2	17·4	0·0700	11·3	4·294	SF
206s	XGS284Z002	3·7	17·7	0·0988	7·6		AGN(abs)
207s	XGS206Z038	0·9	19·2	0·2424	203·4		AGN(abs)
207s	XGS208Z145	5·2	14·1	0·0229	4·7	0·597	SF
207s	TGS207Z011	0·2	14·2	0·0355	55·0		AGN(em)
218s	XGS217Z158	3·4	14·4	0·0207	2·5	0·416	SF
218s	TGS218Z173	3·4	18·6	0·0914	8·9		AGN(em)
218s	XGS219Z089	4·5	18·7	0·2497	59·7		AGN(abs)
219s	TGS219Z142	7·3	17·1	0·1245	8·5		AGN(abs)
220s	XGS221Z290	5·1	19·1	0·2480	7·7		AGN(E+[OIII]em)
220s	TGS220Z015	0·8	19·3	0·2630	12·5		AGN(E+[OIII]em)
220s	TGS220Z009	7·9	18·7	0·2306	3·1		AGN(E+[OII]em)
220s	TGS220Z022	2·8	15·6	0·0575	6·4	0·574	SF
220s	TGS220Z097	3·0	14·3	0·0204	5·4	0·953	SF
220s	TGS220Z128	6·7	18·9	0·1306	3·2		AGN(em)
232s	TGS232Z060	7·6	16·8	0·0590	3·2	0·324	SF
232s	TGS232Z156	5·1	19·3	0·2446	6·1		AGN(abs)
233s	XMS232Z027	6·3	13·2	0·0066	9·8	2·229	SF
233s	TGS233Z084	7·6	18·4	0·0648	3·8		AGN?([OIII]em)
233s	TGS233Z196	7·2	18·3	0·1030	2·2		AGN(abs)
234s	TGS234Z066	1·8	18·9	0·1512	25·2		AGN(em)
234s	TGS234Z197	6·1	17·9	0·1092	21·1		AGN(abs)
234s	TGS234Z186	7·4	18·0	0·1393	4·6		AGN(abs)
234s	TGS234Z027	2·3	14·5	0·0235	9·5	1·079	SF
235s	TGS235Z125	2·6	14·8	0·0243	9·6	0·932	SF
235s	XGS160Z339	1·3	18·6	0·1186	7·1		AGN(abs)
236s	TGS236Z095	1·8	15·4	0·0237	4·6	0·558	SF
236s	TGS236Z091	4·7	17·0	0·0552	3·3	0·251	SF
236s	TGS236Z065	2·3	17·6	0·1420	9·8		AGN(abs)
236s	TGS236Z194	4·7	15·5	0·0237	4·0	0·490	SF
236s	TGS236Z171	3·7	18·5	0·1648	7·0		AGN(abs)
237s	TGS237Z119	3·0	14·6	0·0419	5·7	0·452	SF
238s	TGS238Z241	1·6	18·2	0·2214	10·7	0·918	SF?(orAGN?)
238s	TGS238Z206	9·7	18·1	0·0008	15·6		Galacticstar
238s	TGS238Z047	3·3	16·5	0·0215	5·3	0·741	SF
238s	TMS238Z180	6·9	17·2	0·1255	3·1	0·187	SF
238s	TGS238Z036	9·6	15·0	0·0203	2·8	0·251	SF
239s	XGS238Z030	3·1	17·2	0·0653	5·5	0·482	SF
239s	TGS239Z196	8·6	14·8	0·0219	3·5	0·301	SF
239s	TGS239Z089	5·4	18·8	0·2216	4·3		SF?
239s	TGS239Z061	1·6	18·9	0·1580	3·3		AGN?
240s	TGS240Z082	0·5	17·7	0·1269	11·0		AGN(abs+[NII]em)
240s	TGS240Z211	0·6	18·2	0·1395	42·1		AGN(abs+[NII]em)
240s	TGS240Z013	0·4	18·9	0·2238	3·3		AGN(abs+[OIII]em)
241s	TGS241Z101	1·8	17·8	0·1276	12·7		AGN(abs)
313s	TGS313Z081	4·2	17·7	0·1220	105·8		AGN(abs+Hαem)
313s	TGS313Z100	7·9	17·1	0·1474	17·0		AGN(abs+Hαem)
314s	TGS314Z122	0·9	17·7	0·1440	98·1		AGN(abs)
314s	TGS314Z110	3·0	17·4	0·0820	5·1		AGN(abs)
314s	TGS314Z116	5·3	19·3	0·2355	8·2		AGN(abs)
314s	TMS314Z092	3·1	19·2	0·2134	13·2		AGN(abs)
318s	TGS318Z046	5·8	18·5	0·1544	4·9		AGN(abs)
318s	TGS318Z156	6·9	18·3	0·0687	2·8	0·496	SF
319s	TGS319Z013	2·1	18·7	0·1224	4·2		AGN(abs)
216n	TGN216Z011	2·2	18·8	0·1395	9·8		AGN(abs)
216n	TGN216Z148	6·1	17·9	0·0832	4·1		AGN(abs)
218n	TGN218Z083	5·4	18·1	0·1934	2·8		SF
218n	TGN218Z230	3·1	15·9	0·0201	3·3	0·379	SF

Table 2. (*Continued*)

Field	ID	Offset (arcsec)	$B(J)$ (mag)	z	$S_{1\cdot4}$ (mJy)	IRAS S_{60} (Jy)	Spectral class
218n	TGN218Z228	2·8	17·0	0·0652	10·6		AGN(abs)
218n	XGN219Z136	1·8	19·4	0·1980	7·0		AGN(abs)
220n	TGN220Z065	8·3	17·3	0·0492	4·4	0·287	SF
220n	TGN220Z258	1·4	17·2	0·0607	14·8		AGN(abs)
222n	TGN222Z132	3·8	16·7	0·0505	3·5		SF?
222n	XGN221Z023	2·9	14·3	0·0188	7·8		SF?
222n	TGN222Z108	0·8	16·1	0·0571	3·3		AGN(abs+[NII]em)
222n	TGN222Z318	3·6	16·1	0·0528	12·2		AGN(abs)
222n	TGN222Z218	0·6	19·0	0·2178	5·1		AGN(em)
231n	TGN231Z143	8·7	15·5	0·0314	2·9	0·276	SF
231n	TGN231Z068	1·6	18·8	0·1837	5·6		AGN(em)
231n	TGN231Z211	5·5	16·4	0·0671	2·8		AGN(em)
239n	TGN239Z017	8·0	18·4	0·1154	5·1		AGN(abs+Hα)
239n	TGN239Z013	0·6	17·9	0·1070	105·0		AGN(abs+Hα)
239n	TGN239Z061	5·3	17·5	0·0554	3·3		SF?
239n	TGN239Z082	9·6	18·8	0·1412	2·8		SF
239n	XGN238Z202	0·9	19·3	0·1602	46·3		AGN?(em)
239n	TGN239Z221	2·8	17·4	0·0430	4·8	0·626	SF
239n	TGN239Z171	1·4	18·2	0·1219	2·6		AGN(abs+[NII])
239n	TGN239Z158	9·8	18·3	0·1289	52·5		AGN(abs)
239n	TGN239Z172	3·7	16·2	0·0459	9·5	0·931	SF, interacting?
240n	TGN240Z127	8·1	17·0	0·0554	2·4		SF??
240n	XGN309Z233	4·6	17·9	0·0677	3·9		SF?
240n	TGN240Z277	0·6	16·9	0·0766	6·4		AGN(abs)
240n	TGN240Z219	8·5	19·3	0·1216	5·1		SF?

source can be identified with each optical galaxy). Thus about 27 chance coincidences are expected in a total of 8362 galaxies (see column 5 of Table 1). This calculation ignores the known clustering of galaxies on the sky, although this will only invalidate the result if there is significant clustering on scales comparable to the identification range of 15 arcsec, or if there are substantial differences between the spatial distribution of radio-loud and quiet galaxies. We believe these effects are unlikely to give an error of more than 10%.

The results suggest that candidate matches with an offset of up to 10 arcsec are highly likely to be real associations. We therefore use a simple 10 arcsec cutoff in the radio–optical position difference for the analysis which follows. This gives us 99 radio-detected galaxy matches in the thirty 2dF fields. It also means that we have probably omitted about a dozen real identifications with larger offsets, but this is not a problem here since our aim is to make a first qualitative exploration of the faint radio galaxy population.

4 Two Kinds of Radio Source: AGN/SF Classification

We classified each matched galaxy as either 'AGN' or 'star-forming' (SF) based on its 2dF spectrum. The 'AGN' galaxies have either a pure absorption-line spectrum like that of a giant elliptical galaxy, or a stellar continuum plus nebular emission lines such as [OII] and [OIII] which are strong compared with any Balmer-line emission. Some of the emission-line AGN have spectra which resemble Seyfert galaxies.

The 'SF' galaxies are those where strong, narrow emission lines of Hα and (usually) Hβ dominate the spectrum. They include both nearby spirals and more distant IRAS galaxies. Figure 1 shows examples of spectra we classified as AGN, Seyfert and SF. Note that in this classification scheme, 'AGN' may simply denote the presence of radioillustrator emission, with no obvious optical signature. The origin of radio emission in the AGN and SF galaxies is believed to be quite different (e.g. Condon 1989), arising from non-thermal processes related to a central massive object in the AGN galaxies and from processes related to star formation (including supernova remnants, HII regions, etc.) in the SF galaxies.

We are confident that this simple 'eyeball' classification of the 2dF spectra allows us to separate the AGN and SF classes accurately. Jackson & Londish (2000) measured several emission-line ratios (including [OIII, $\lambda5007$]/Hβ, [NII, $\lambda6584$]/Hα, [OI, $\lambda6300$]/Hα and [SII, $\lambda\lambda6716,6731$]/Hα) for most of the galaxies studied here and plotted them on the diagnostic diagrams of Veilleux & Osterbrock (1987). They found that the 'eyeball' classifications and line-ratio based classifications agreed more than 95% of the time, and hence that 'eyeball' classifications can be used with confidence to analyse large samples of 2dF spectra.

Most of the 2dF spectra are of impressively good quality. However, of the 98 spectra we examined (one galaxy was not actually observed by the 2dFGRS), nine had such a low signal-to-noise ratio that we were
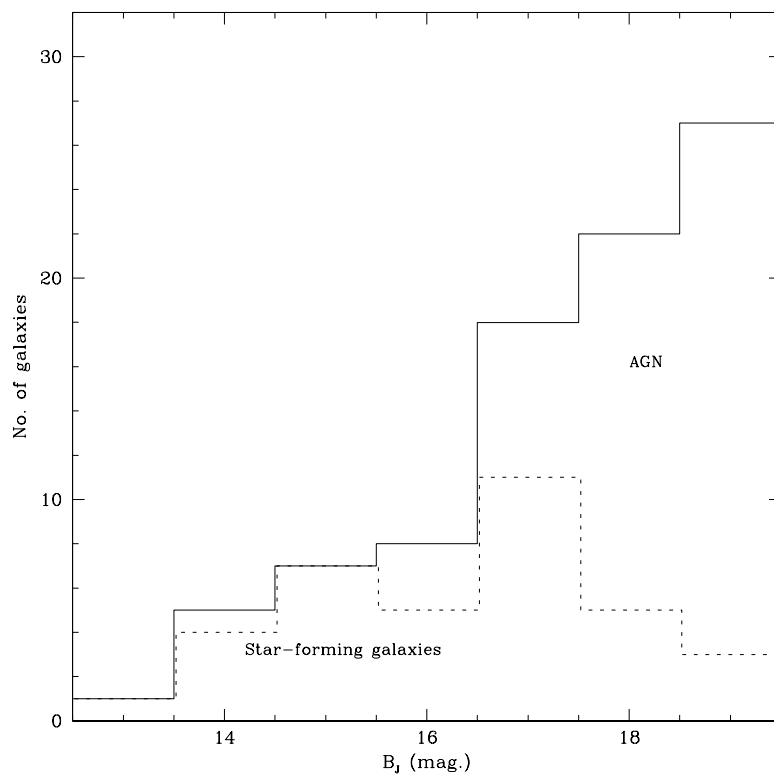
Figure 2—Distribution of the star-forming and AGN galaxies in apparent magnitude. Note that star-forming galaxies dominate at the bright end ($b_J < 17$ mag.), while most of the fainter galaxies have AGN spectra.
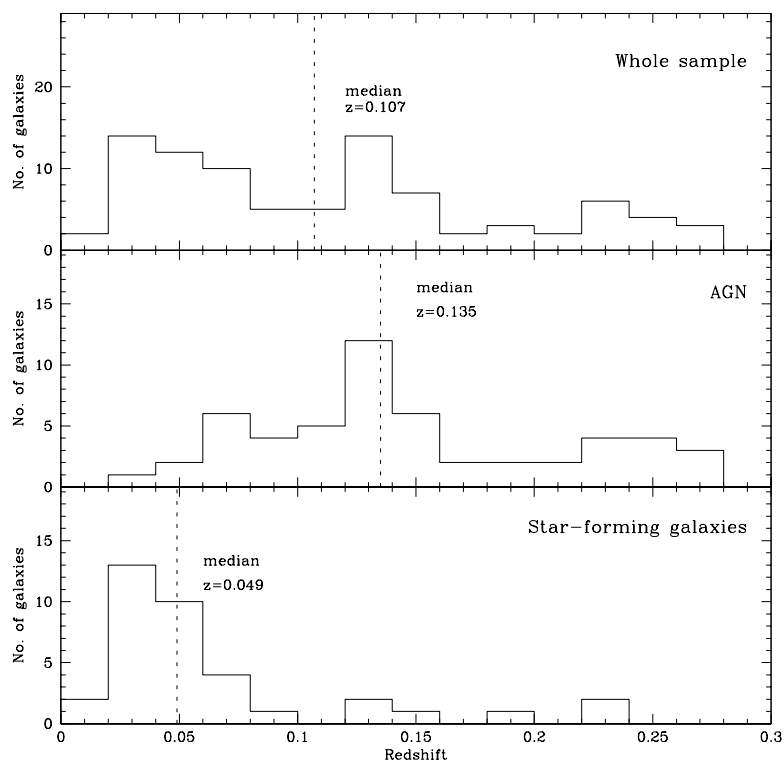

Figure 3—Redshift distribution of the AGN and star-forming galaxies, and of the whole sample. Most of the star-forming galaxies are relatively nearby, though some extend out to redshifts of $0 \cdot 25$. The AGN galaxies are a more distant population, with a median redshift almost three times that of the star-forming galaxies.
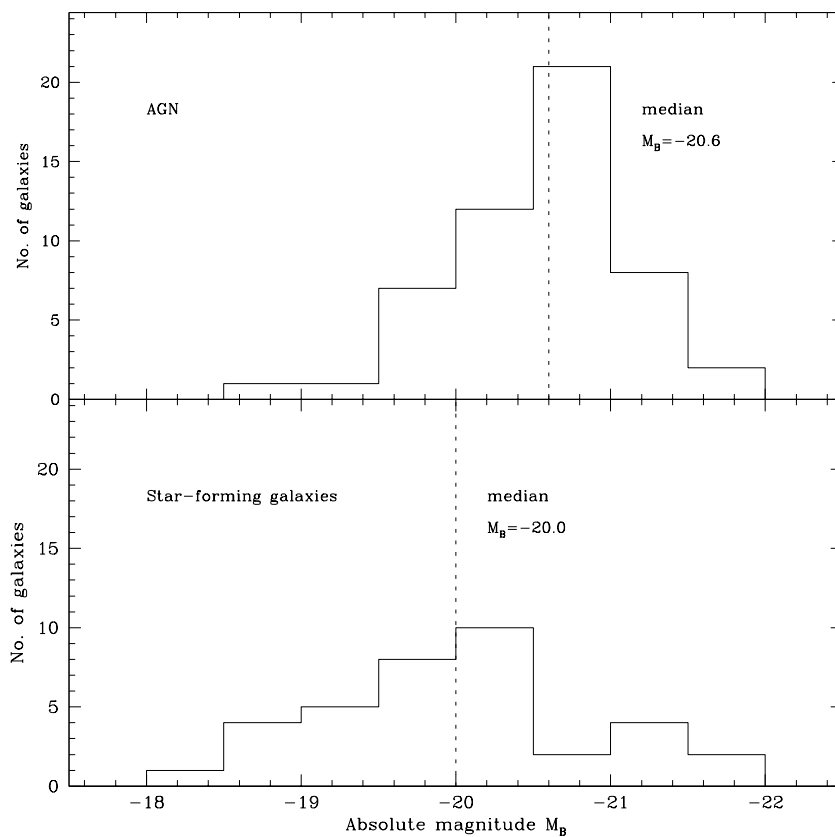
Figure 4—Absolute magnitude histograms for the AGN and star-forming galaxies. The AGN spectra are typically found in luminous optical galaxies, while the star-forming galaxies span a much wider range in optical luminosity.
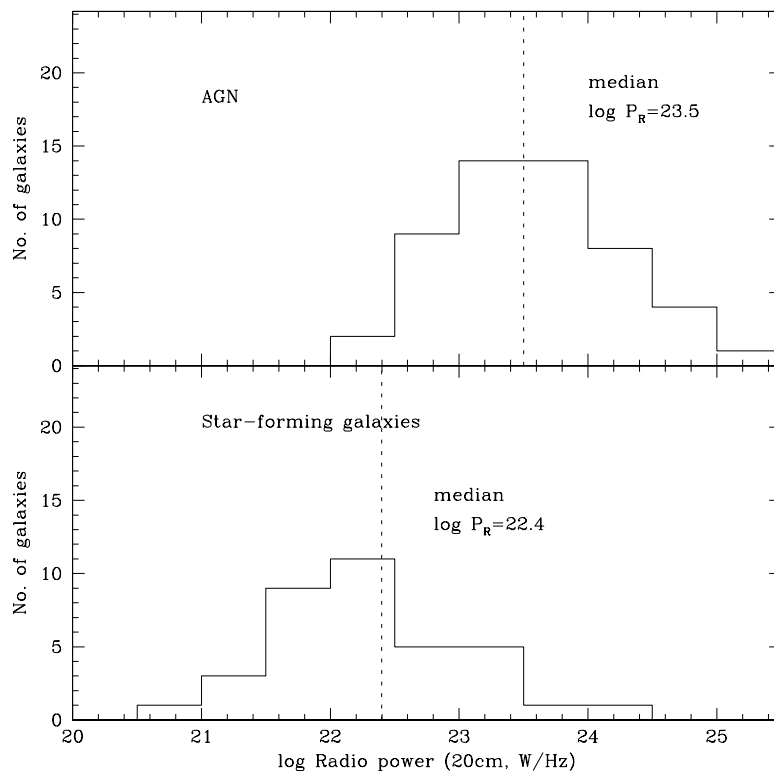

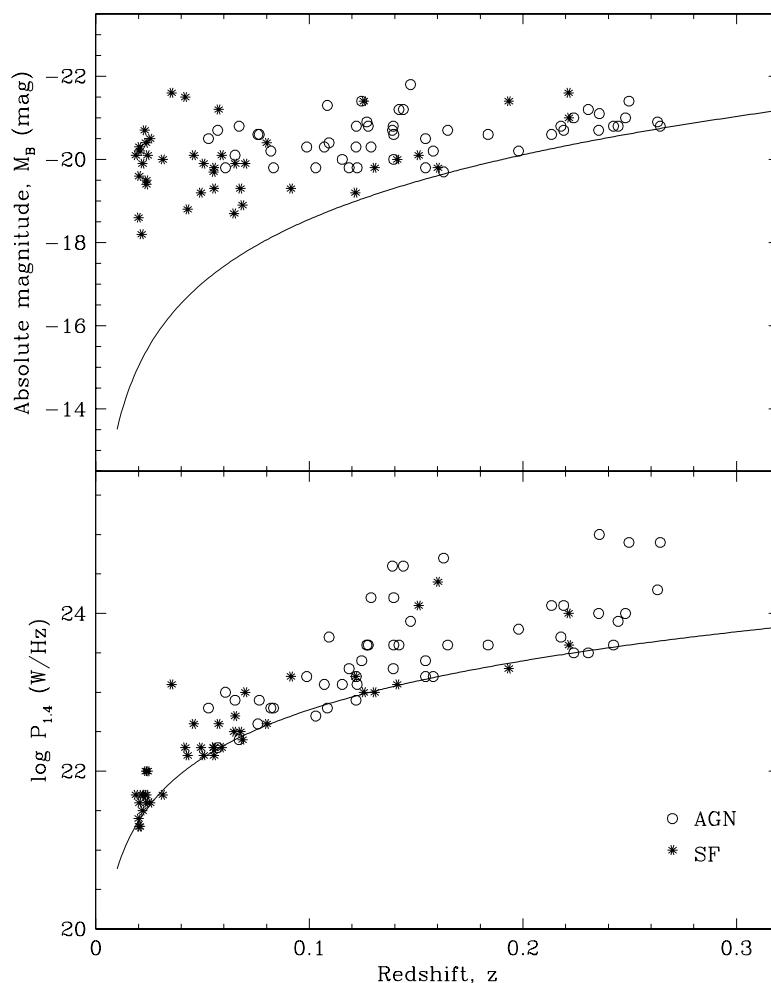**Figure 5**—Histograms of radio power for the AGN and star-forming galaxies.

Figure 6—Plots of radio power (*bottom*) and optical luminosity (*top*) versus redshift for AGN (shown by open circles) and SF (shown by stars) galaxies. The curve in each plot shows the radio and optical limits of the NVSS and 2dFGRS respectively—galaxies below these curves will drop out of our sample.

unable to classify the spectrum. One other object appeared to be a Galactic star. We were therefore left with 88 good-quality 2dF spectra of candidate radio matches with an offset $D < 10$ arcsec. Of these 88 galaxies, 36 (41%) were classified as SF and 52 (59%) as AGN. One galaxy classified as SF had an emission-line spectrum which resembled an AGN, but was also detected as an IRAS source at 60 μm. This may be a genuinely composite object. Table 2 lists the matched galaxies, their spectral classification, 1·4 GHz radio continuum flux density, apparent magnitude and redshift. A more quantitative spectral classification using diagnostic emission-line ratios will be presented in the forthcoming paper by Jackson & Londish (2000).

Figures 2 and 3 show the distribution of AGN and SF classes in apparent magnitude and redshift respectively. There is a clear segregation in apparent magnitude: most galaxies brighter than about b_J = 16·5–17 mag. fall into the star-forming (SF) class, while the AGN class dominates the population fainter than $b_J \sim 17$. This reflects strong differences

in the global properties of the two classes as well as the radio and optical flux limits of the NVSS and 2dFGRS. The AGN galaxies are typically more distant than the SF galaxies (by about a factor of 3—see Figure 3), and more luminous both optically and in radio power (see Figures 4 and 5). We know that the SF galaxies continue to large redshifts and to very faint optical magnitudes (e.g. Benn et al. 1993), but these galaxies quickly drop out of our sample because of the 2–3 mJy limit of the NVSS in radio flux density. Similarly, we know that the AGN galaxies extend to much higher redshifts than probed by the 2dFGRS, but these distant AGN galaxies will be fainter than the $b_J = 19·4$ mag. optical limit of the 2dFGRS. Figure 6 shows plots of radio power and optical luminosity versus redshift for the AGN and SF classes—the curves correspond to the survey completeness limits of 3·5 mJy and 19·4 mag. for the NVSS and 2dFGRS respectively. Galaxies below these lines will be excluded from our sample. Note that most of the SF galaxies are weak radio sources, lying close to the NVSS cutoff
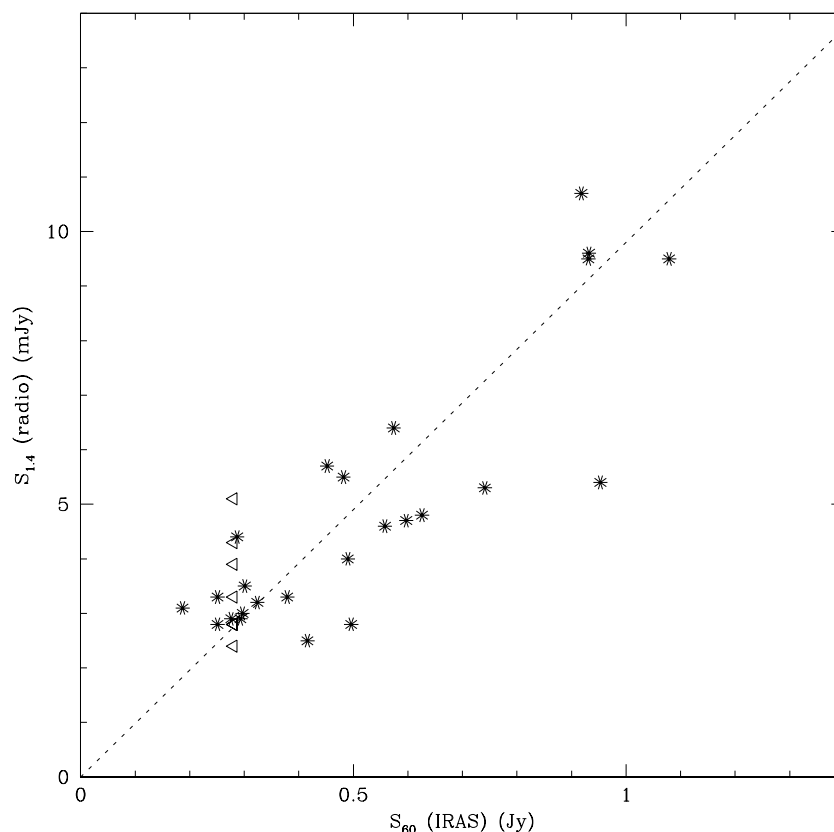
Figure 7—Comparison of radio ($1 \cdot 4$ GHz) and IRAS far-infrared (60 μm) flux density for the radio-detected star-forming galaxies in the 2dFGRS. The dotted line is for $S_{60\mu m} = 100 S_{1 \cdot 4\,\mathrm{GHz}}$. Of the nine SF galaxies in Table 2 which lack IRAS data, two lie in regions not observed by IRAS. For the remaining seven we show (open triangles) upper limits of $0 \cdot 28$ Jy at 60 μm, corresponding to the limits of the IRAS Faint Source Catalogue.

at all redshifts, while most of the AGN galaxies lie well above the radio limit but start to drop below the optical cutoff at redshifts above $0 \cdot 15$.

5 Matches with IRAS Sources

We expect many of the SF radio sources to be IRAS detections, based on the well-known correlation between radio continuum and far-infrared (FIR) luminosities (e.g. Wunderlich, Klein & Wielebinski 1987; Condon, Anderson & Helou 1991). For spiral galaxies, $S_{60\mu m} \sim 100 S_{1 \cdot 4\,\mathrm{GHz}}$ (e.g. Condon & Broderick 1988; Rowan-Robinson et al. 1993), so NVSS should detect most galaxies in the IRAS Faint Source Catalog (which has a flux density limit of $0 \cdot 28$ Jy at 60 μm).

Of the 36 galaxies classified as SF in Table 2, two (TGN222Z132 and XGN221Z023) lie in the 3% of the sky which has no IRAS coverage (Beichman et al. 1985). Of the remaining 34 galaxies, 27 (i.e. 79%) are detected at 60 μm in the IRAS Point Source Catalog or Faint Source Catalog (FSC). Figure 7 compares the radio continuum ($1 \cdot 4$ GHz) and IRAS (60 μm) flux densities for these galaxies (for galaxies undetected by IRAS we show an upper limit of $0 \cdot 28$ Jy, corresponding to the completeness level of the FSC). If we exclude one galaxy with anomalously

strong 60 μm emission as discussed below, the mean FIR–radio ratio $Q_{60} = S_{60\mu m}/S_{1 \cdot 4\,\mathrm{GHz}}$ for the IRAS-detected galaxies is 112±8, i.e. close to that derived from other studies.

One galaxy (TMS206Z015) has an unusually high value of $Q_{60} = 380$, with much stronger FIR emission than would be expected from the radio continuum flux density. The most likely explanation is confusion in the IRAS beam, since this galaxy lies in a group and appears to be interacting with a companion.

6 Conclusions

Based on a study of thirty fields from the 2dF Galaxy Redshift Survey, we find that about $1 \cdot 5\%$ of 2dFGRS galaxies brighter than $b_J < 19 \cdot 4$ magnitude are candidate identifications for $1 \cdot 4$ GHz NVSS radio sources. Of these about 80–85% will turn out, after closer examination, to be 'real' associations. Thus if the whole 2dFGRS contains 250,000 galaxies, we expect to identify about 4000 candidate matches with NVSS by the time the 2dFGRS is complete. About 60% of these galaxies will be AGN (radio galaxies and some Seyferts) and 40% star-forming galaxies. For galaxies south of declination $-30°$, we will also have 843 MHz radio flux density measurements from the Sydney University Molonglo Sky Survey

(SUMSS; Bock, Large & Sadler 1999), and will be able to measure radio spectral indices.

The final sample will be by far the largest (and most homogeneous) sample of radio-galaxy spectra ever obtained, and will allow us to study both the AGN and starburst radio populations out to a redshift $z \sim 0 \cdot 3$, and to look for evidence of evolution over this redshift range. As the present paper goes to press, the 2dF Galaxy Redshift Survey is 20% complete and our sample has already grown to more than 700 galaxies. This larger sample will be analysed in more detail in a forthcoming paper.

Acknowledgments

We thank the 2dF Galaxy Redshift Survey team for allowing us early access to their data. We also acknowledge the essential contribution of the many people, at the AAO and elsewhere, who have contributed to the building and operation of the 2dF facility. Finally, we thank the two anonymous referees of this paper for their careful reading and helpful suggestions.

The IRAS flux densities quoted in Table 2 were obtained from the NASA Extragalactic Database (NED).

References

Becker, R. H., White, R. L., & Helfand, D. J. 1995, ApJ, 450, 599
Beichman, C. A., Neugebauer, G., Habing, H. J., Clegg, P. E., & Chester, T. J. 1985, IRAS Explanatory Supplement, JPL
Benn, C. R., Rowan-Robinson, M., McMahon, R. G., Broadhurst, T. J., & Lawrence, A. 1993, MNRAS, 263, 98
Bock, D. C.-J., Large, M. I., & Sadler, E. M. 1999, AJ, 117, 1578
Colless, M. 1999, Phil. Trans. R. Soc. London A, 357, 105 (astro-ph/9804078)
Condon, J. J. 1984, ApJ, 287, 461
Condon, J. J. 1989, ApJ, 338, 13
Condon, J. J. 1992, ARA & A, 30, 575
Condon, J. J., & Broderick, J. J. 1988, AJ, 96, 30
Condon, J. J., Anderson, M. L., & Helou, G. 1991, ApJ, 376, 95
Condon, J. J., Cotton, W. D., Greisen, E. W., Yin, Q. F., Perley, R. A., Taylor, G. B., & Broderick, J. J. 1998, AJ, 115, 1693
Cress, C. M., Helfand, D. J., Becker, R. H., Gregg, M. D., & White, R. L. 1996, ApJ, 473, 7
Folkes, S., et al. 1999, MNRAS, 308, 459
Jackson, C. A., & Londish, D. M. 2000, PASA, submitted
Lewis, I. J., Glazebrook, K., & Taylor, K. 1998, SPIE Proc., 3355, 828
Maddox, S. J. 1998, in Large Scale Structure: Tracks and Traces, Proc. 12th Potsdam Cosmology Workshop, ed. V. Müller et al. (Singapore: World Scientific), p. 91 (astro-ph/9711015)
Magliocchetti, M., Maddox, S., Lahav, O., & Wall, J. V. 1998, MNRAS, 300, 257
Rengelink, R. B., Tang, Y., de Bruyn, A. G., Miley, G. K., Bremer, M. N., Röttgering, H., & Bremer, M. A. R. 1997, A&AS, 124, 259
Rowan-Robinson, M., Benn, C. R., Lawrence, A., McMahon, R. G., & Broadhurst, T. J. 1993, MNRAS, 263, 123
Smith, G., & Lankshear, A. 1998, SPIE Proc., 3355, 905
Veilleux, S., & Osterbrock, D. A., 1987, ApJS, 63, 295
Windhorst, R. A., Miley, G. K., Owen, F. N., Kron, R. G., & Koo, D. C. 1985, ApJ, 289, 494
Wunderlich, E., Klein, U., & Wielebinski, R. 1987, A&AS, 69, 487